Analytical Methods

RSC Publishing

PAPER

View Article Online
View Journal | View Issue

Cite this: *Anal. Methods*, 2013, **5**, 6925

Investigation of blood vessels in glioblastoma at a micrometric scale: a comparative study by synchrotron and conventional micro-FTIR†

Katia Wehbe,‡[a] Adrian Travo,‡[b] Sandrine Eimer,[c] Gianfelice Cinque,[a] Emmanuelle Barron,[b] Gérard Déléris[b] and Isabelle Forfar*[b]

Received 27th August 2013
Accepted 8th October 2013

DOI: 10.1039/c3ay41449c

www.rsc.org/methods

Glioblastoma, the most malignant brain tumor in humans, is characterized by being severely angiogenic and an increase in vascularization generally worsens the prognosis of patients. Finding the best approach to characterize glioma blood vessels (BVs) is very important in view of helping to determine any specific biomolecular markers of these tumors. In previous work by conventional FTIR spectroscopy we were able to discriminate some molecular markers in order to differentiate between normal and tumor BVs in glioma tissue sections. The aim of the present study was to assess whether FTIR microspectroscopy using a synchrotron radiation (SR) source could provide advantages over a classical globar IR source for detailed spectral analysis on such small features like micro-BVs. Using chemometric analysis such as PCA and HCA, the results show that a high brilliant SR beam provides a very satisfying quality signal compared with the globar source to study spectral images for relevant analysis of glioma big and micro-BVs and determination of subtle molecular markers characterizing them from the surrounding tissue.

Introduction

Being the most malignant brain tumor in patients, glioblastoma accounts for up to 50% of all gliomas in adult patients.[1] Significant intra-tumoral heterogeneity is present in glioblastoma, *i.e.* cells of an individual glioma may differ in their morphology, genetics and biological behavior.[2] Moreover, glioblastoma are among the most angiogenic human tumors, thus endothelial proliferation is a hallmark of the disease.[3,4] Angiogenesis, or in other terms sprouting of new blood vessels (BVs) from pre-existing ones, plays an important role as a major prognostic factor in this type of tumor. Tumor BVs are structurally and functionally abnormal, and contribute to an unfavourable micro-environment leading to a more malignant phenotype. Currently, histopathology of excised tissue using hematoxylin–eosin (HE) staining is the gold standard for examination of these tumors. This is usually limited by subjective interpretation of pathologists due to the tumor heterogeneity, therefore there is a high priority for the development of molecular based imaging techniques for histopathology examinations. Finding the best approach to characterize glioma blood vessels (BVs) is very important in view of helping to determine any specific biomolecular markers of these tumors.

Infrared (IR) imaging and Fourier transform IR (FTIR) spectroscopy allow for both qualitative and quantitative analyses of the basic components of biological tissues. Following the recent literature,[5–9] the IR technique is quickly approaching its utility as an additional tool for molecular histopathology by detecting subtle chemical changes in human tissue samples. FTIR imaging using a conventional source has been successfully used to detect macro-alteration of molecular structure *e.g.* protein secondary structure of BVs in glioma tumors at different stages.[10] The technique was also able to highlight molecular markers differentiating between normal and tumor BVs in xenografted as well as human brain tumors.[11] Few other studies used FTIR imaging to discriminate between healthy and tumor tissues on examining large areas (field of view over a few millimeters).[12–14]

In the field of so-called "Spectral Histopathology"[15] an important step of interpreting the acquired images is the application of chemometrics spectral data processing. Chemometric analysis is a robust approach allowing full exploitation of IR maps, and presents the ability to characterize subtle but significant spectral changes in a large dataset.[16] Consequently, it permits identification of subtle spectral features related to a

[a]*Diamond Light Source Ltd, Harwell Science and Innovation Campus, Didcot, OX110DE, UK. E-mail: Katia.Wehbe@Diamond.ac.uk; Fax: +44 (0) 1235 778 448; Tel: +44 (0) 1235 778 498*

[b]*CNRS FRE 3396 (Pharmacochimie), UFR de Pharmacie Université Bordeaux, Bordeaux, France. E-mail: isabelle.forfar@u-bordeaux2.fr; Fax: +33 557571352; Tel: +33 557571559*

[c]*Department of Pathology, Pellegrin University Hospital, Bordeaux, France. E-mail: sandrine.eimer@chu-bordeaux.fr; Fax: +33 (0)5 56 79 60 88; Tel: +33 (0)5 56 79 56 02*

† In memory of Professor Gérard Déléris.

‡ These authors contributed equally to this work.

disease state in a very large and complex spectral dataset. It has been demonstrated[17–19] that FTIR imaging of tumor tissue combined with advanced chemometrics can highlight significant spectral changes related to molecular inter- and intra-tumor heterogeneity not detectable by conventional HE or immuno-histochemistry (IHC) staining.

Conversely, when studying small structures and/or substructures of small samples on a micrometric scale, such as a specific part of a tissue section like micro-BVs, benchtop FTIR spectrometers used in most laboratories present intrinsic limitations. The microanalysis approach at high spatial resolution is significant only if combined with sufficient spectral quality for further analysis, and this is the drawback of conventional broadband sources. Nowadays, with the usage of synchrotron radiation (SR), FTIR microspectroscopy can overcome most of such limitations of conventional IR systems, namely by providing diffraction limited (*i.e.* highest optically attainable) spatial resolution and enhanced signal to noise ratio (SNR) in the whole IR fingerprint region.[20,21] SR sources provide an extremely brilliant IR beam that can be used for different applications especially in the biomedical field giving high spatial resolution and high SNR.[22]

In a previous study, Ali *et al.*[1] used SR-IR microspectroscopy to detect changes in glioblastoma tissue samples due to tumor progression but, to our knowledge, there is no report in the literature of any study on glioma tumor BV characterization on a micrometric scale by SR-IR microspectroscopy. We present here a preliminary comparative study of IR spectral data acquired on human glioblastoma tissue sections with both SR and globar sources to assess if SR sources could provide practical advantages over conventional sources when analyzing particularly BVs of different sizes.

Materials and methods

Human tissue samples

Two brain tumor specimens were obtained from patients undergoing neurosurgery and provided from Bordeaux University Hospital Center in collaboration with the pathology department. Informed consent of the patient was obtained. All experiments in this work were carried out in compliance with the relevant laws and institutional guidelines in France (revised 2011 bioethics laws), and have been approved by the institutional committee. Fresh samples were frozen in liquid nitrogen immediately after tumor resection to perform cryosectioning. A 20 μm thick section from each specimen was put onto an IR-transparent double polished silicon window for FTIR analysis. Pathological diagnosis was performed from experienced pathologists' observations of additional HE sections and samples were diagnosed to be gliomas grade IV according to WHO (World Health Organization) classification.

FTIR spectral imaging acquisition

Two BVs of different sizes were chosen from the two sections: a big BV of about 90 μm diameter and a micro-BV of about 10 μm diameter. Spectral images were collected in transmission mode using a Bruker Hyperion 3000 microscope available at the MIRIAM beamline at Diamond Light Source, UK.[23] The imaging system is equipped with a liquid nitrogen cooled MCT detector. Spectra were acquired using both SR and thermal (globar) IR sources in the range of 4000–400 cm^{-1} at 4 cm^{-1} spectral resolution using the 36× objective. For the big BV image acquisition (about 140 min of acquisition time), the aperture size was set to 10 × 10 μm^2 at the sample, and oversampling 2 times (by 5 μm step size) accumulating 32 scans in normal mode. For the micro-BV image acquisition (about 40 min acquisition time), 5 × 5 μm^2 aperture was used oversampling by 3 μm step size and 128 scans were accumulated in confocal mode. By matching the 36× condenser slits to 5 × 5 μm^2 like the objective aperture size, the diffraction limited spatial resolution is achieved in confocal mode.[24]

FTIR data processing

Data processing was performed using the "3D" extension of OPUS 7.0 software (Brüker Optics, Ettlingen-Germany). All data from spectral images were baseline corrected using the concave rubber band algorithm (using 10 iterations and 64 points). All uni- and multivariate analyses were performed in the 900–3200 cm^{-1} spectral range. To generate the peak ratio, peak areas were calculated using integration method B. The SNR was calculated on the average spectrum of each BV map as the ratio of the transmission signal *versus* root mean square value of the noise within the range 2700–2400 cm^{-1} (n.b.: region free from water absorption bands).

Principal component analysis (PCA). Principal component analysis (PCA) is an unsupervised multivariate analysis method that linearly decomposes the spectra in a dataset of "independent Principal Components" (PCs) or "loading vectors", which are based on the maximal variance of spectra. PCs intrinsically account for less and less of the variance in the dataset, thus the first few PCs are sufficient to describe most of the information contained in the whole set. The "quantity" of each PC in the given spectra is named "Scores" (S), and the unique score associated with each spectrum is used to classify and/or group spectral data. Each spectrum of a dataset is characterized by the sum of all calculated PCs weighted by their respective scores:

$$Sp = PC_1 \times S_1 + PC_2 \times S_2 + PC_3 \times S_3 + \ldots + PC_n \times S_n \quad (1)$$

where Sp is a given spectrum of a spectral dataset, PC corresponds to the loading vector, S corresponds to PC scores, and n corresponds to the number of calculated PCs.[16,25]

Hierarchical cluster analysis (HCA) and pseudo-color image construction. HCA is a "hard" clustering method, *i.e.* spectra may belong to a given cluster or not. All data points, *i.e.* absorbance values, from individual spectra are compared based on their Euclidean distance to the average of the spectra included in the database using Ward's algorithm. The calculation of distances leads to the classification of spectra in the form of a dendrogram. The final partition of spectra into classes is defined by "cutting" the dendrogram. While the clustering process is completely unsupervised, this step is subjective and defines the number of classes, which will appear in the cluster

image. Cluster image assembly on the basis of HCA follows the simple idea of assigning a distinct color to all spectra in one cluster. Since each spectrum of a mapping experiment has a unique spatial x, y position in the map, false-color images can be generated by plotting specifically colored pixels as a function of the spatial coordinates.[16,26]

Results and discussion

Glioblastomas are particularly characterized by an endothelial proliferation. Extensive angiogenesis and markedly abnormal vessels are hallmarks of glioblastoma, thus the tumor-associated blood vessels have a major impact on glioma pathology.[27] In order to improve the analysis of blood vessels highly specific to glioma (grade IV) tissue it is necessary to get better resolved IR imaging of the vessels. On purpose, we carried out experiments in a comparative way using two IR sources. The analysis required an aperture well-appropriated to the scale of the studied BV sample as well as fulfilling the requirement of sufficient SNR for successive spectral analysis by PCA and HCA. Therefore the aperture size was 10 × 10 μm^2 for the big BV (about 90 μm diameter), and 5 × 5 μm^2 for the micro-BV (about 10 μm diameter). The globar source was used as a conventional IR light source, which allows us to work with a good SNR using an aperture set to 20 μm or above.[28] On the other hand, the study was also performed on using the SR source, which can be 100–1000 times brighter than a thermal source.[29] Although the overall mid-IR power from a SR source is less than that from a globar source, it is the synchrotron's brightness that gives it a major advantage for microspectroscopy. Therefore, the brightness of the SR source offers a real advantage when performing mid-IR spectroscopy microanalysis.[30,31]

As mentioned above, it is widely recognized that chemometrics approaches like PCA, MCR-ALS (multivariate curve resolution-alternating least squares) or clustering, such as hierarchical or K-means clustering, are the methods of choice for full exploitation and optimal studies of a large spectral dataset such as spectral images.[1,12,16–18,25,26,32] However, preliminary evaluation of spectral data by a classical curve integration ratio between spectral ranges assigned to principal constituents of the tissue still presents some interest. This permits quick evaluation of the variation of relative amounts of lipid, protein and carbohydrate contents depending on main tissue structures. Consequently, we firstly present a comparison of pseudo-color spectral images of the big and micro-BVs chosen from the two glioblastomas depending on the used IR source for acquisition (Fig. 1). These pseudo-color images were constructed based on the protein to lipid ratio (1500–1700/2800–3000 cm^{-1}) in each spectrum of the datasets. This ratio has been previously reported as the first important IR spectral marker to enhance the image contrast in the brain tissue study.[33]

Visible images of studied vessels are shown in Fig. 1A–D. For data acquired on the big BV, the pseudo-color images permit us to accurately delimit the vessel with both globar (Fig. 1B) and SR sources (Fig. 1C). However, the image obtained with the SR source permits us to clearly highlight the sub-structure of the vessel *i.e.* the lumen (central space of the vessel through which the blood flows, lumen diameter in this BV is about 15 μm) much better than the image obtained with the globar source. We can also clearly identify the three layers that form a BV: tunica intima (the innermost layer of endothelial cells), tunica media (the middle thick layer of smooth muscle that is surrounded by a membrane) and tunica externa (the outermost

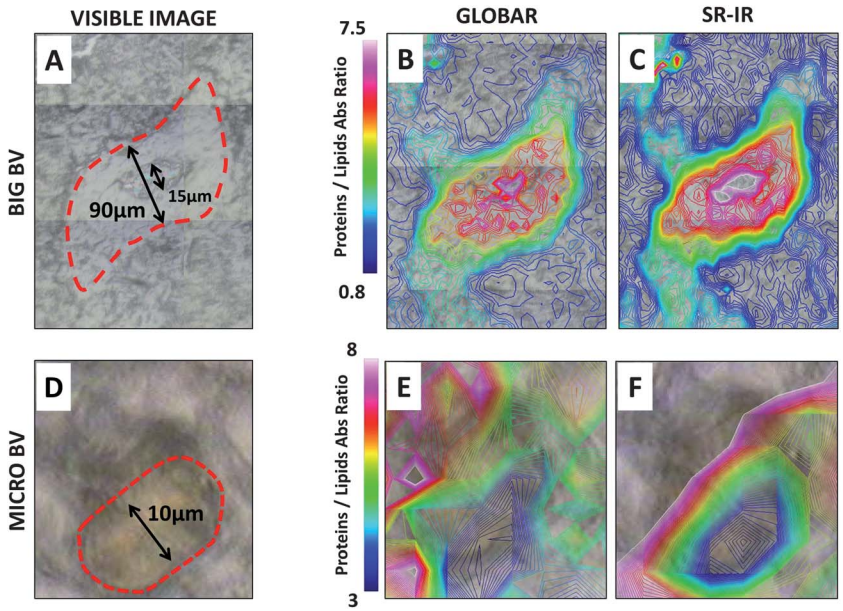

Fig. 1 Representative pseudo-color spectral images of glioma big and micro-blood vessels (BVs) constructed based on the protein/lipid absorbance ratio depending on the used IR source. (A) Visible image of the big BV. (B and C) Corresponding pseudo-color images based on the absorbance ratio of 1500–1700/2800–3000 cm^{-1} from data acquired with the globar and SR source, respectively. (D) Visible image of the micro-BV. (E and F) Corresponding pseudo-color images based on the absorbance ratio of 1500–1700/2800–3000 cm^{-1} from data acquired with the globar and SR source, respectively.

layer consisting of collagen). Concerning data acquired on the micro-BV, there is a remarkable difference between the images acquired with each source. Using the globar source (Fig. 1E), the pseudo-color image appears not to be totally satisfactory because not very well delimiting the area corresponding to the vessel and showing noisy features all over the area. In contrast, when acquired with the SR source using the same acquisition parameters (Fig. 1F), the pseudo-color image corresponds tightly to the visible image, and the blood vessel is well delimited by a uniform transition area. A clearer sub-structure of the BV is shown even the lumen space compared to the globar and to the visible image as well. It is noteworthy to mention that the slight shift (about 5 μm) between the visible image and the IR image (Fig. 1E and F) is in fact due to the visible image being captured in reflection mode since silicon is opaque to the visible and the IR image being acquired in transmission mode. This shift between the two modes due to the difference in optics is accentuated on a small scale hence it is not obvious in the image of the big BV. It should be noted that the calculated SNR appears to be nearly 6.2 times better for the big BV image (5606 *vs.* 895) and 15 times better for the micro-BV image (1921 *vs.* 128) when acquired with a SR-IR source compared to the ones with the globar source. The higher photon flux density released at the sample by the narrowed SR-IR beam enhances the IR signals from the blood vessel restricted within 10 × 10 μm^2 (or lower) aperture slits of the microscope well above the background noise. The difference in the SNR between the two vessel images acquired with the SR (6.2 *versus* 15 times) is due to the different number of scans, *i.e.* less scans accumulated for the big BV image since the map extension would have taken a much longer measurement time if using the same number of scans of the micro-BV image. The higher SNR, which was reached for the micro-BV data using the SR source, is also due to the implementation of the confocal measurement mode. In normal mode the aperture slits from the top limits the spot area which is illuminating the sample. In confocal mode, in addition to the aperture from the top there are also the condenser slits (to be closed matching the aperture size) which also decrease the spot in order to improve the spatial resolution.

We then assessed if common chemometrics processing could provide accurate discrimination of spectral data assigned to BVs from the surrounding tissue for both spectral data acquired with the globar and SR source.

PCA is a well described and widely used an unsupervised chemometric analysis method that permits us to (i) reduce complexity of a dataset, (ii) discriminate different population of spectra and (iii) extract spectral features associated with diseases or cell responses to a particular stimulus.[15,16,25] Moreover, PCA presents the significant advantage to allow improvement of signal quality by removing a part of non-informative component of spectral data such as noise. Fig. 2 presents visible images of the studied vessels and the associated pseudo-color images based on PCA analysis of spectral data. For spectral data acquired on the big BV, only the image constructed based on PC2 scores permits us to match closely the visible image by delimiting the BV from the surrounding tissue without any ambiguity. This is observed for both data acquired with globar and SR sources (Fig. 2B and C). Therefore, this strongly suggests that PC2 loadings contain spectral, *i.e.* biochemical features that characterize the BV and differentiates it from the surrounding tissue. This is in accordance with the basic theory of PCA as the first PC generally expresses the mean of all spectra, whereas the second PC expresses the most significant variations in the dataset.[15] In addition, PC loadings (Fig. 2D) appear to be comparable between the two used sources. Thus, for a relatively large structure, PCA permits us to enhance the globar based signal and to obtain scores-based pseudo-color images of glioma vessels comparable to those obtained with the SR source.

In contrast, for spectral data acquired on the micro-BV in confocal mode, the PC2 score-based image does not permit us to represent the BV accurately when using the globar source

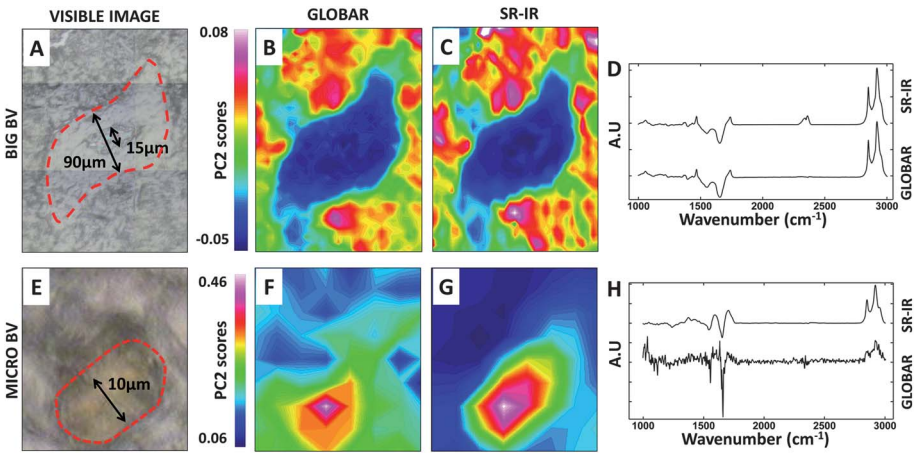

Fig. 2 Representative pseudo-color spectral images of glioma big and micro-BV constructed based on PCA results depending on the used IR source. (A) Visible image of the big BV. (B and C) Corresponding pseudo-color images based on PC2 scores from data acquired with the globar and SR source, respectively. (D) Associated PC2 loadings. (E) Visible image of the micro-BV. (F and G) Corresponding pseudo-color images based on PC2 scores from data acquired with the globar and SR source, respectively. (H) Associated PC2 loadings.

(Fig. 2F). It should be noted that this was the case for all calculated PCs on this dataset. By contrast, the PC2 score image obtained with the SR source permits us to accurately image the micro-BV defining well its limits from the surrounding tissue (Fig. 2G). In this case PC2 loadings (Fig. 2H) present a satisfactory signal quality allowing further extraction of spectral features significantly associated with intra- and inter-tissue biochemical differences especially in the protein to lipid ratio. However, the PC2 loading vector obtained from globar data appears to be noisy, as for all calculated PC loadings in this case, thus not allowing relevant spectral analysis.

HCA is one of the most popular and powerful unsupervised classification methods in the field of biospectroscopy allowing us to group spectra into clusters depending on their "similarity". It allows us to reveal very subtle but significant spectral, *i.e.* biochemical, differences in the studied samples. Fig. 3 presents the visible image of the studied glioma BVs and associated cluster images based on HCA for both data acquired with the globar and SR source. For the cluster image obtained from the big BV using the globar source (Fig. 3B), it is challenging to retrieve any cluster that unequivocally matches with the BV contour and the lumen. This was the case whatever the number of clusters tested. In contrast, for spectral data acquired with the SR source (Fig. 3C), HCA processing permits construction of a cluster image that represents very accurately the BV and its sub-structure. In this case the white cluster corresponds to spectra associated with the lumen, most probably the orange cluster to the internal layers of the BV *i.e.* tunica intima/tunica media, and the green cluster to the external layer of the BV *i.e.* tunica externa which separates it from the surrounding tissue (blue cluster).

Concerning the cluster image obtained from the micro-BV using the globar source (Fig. 3E), it is impossible to retrieve a cluster matching the BV. This was the case whatever the number of clusters tested. By contrast, the cluster image obtained using the SR source (Fig. 3F) presents one cluster that can be unequivocally assigned to the studied vessel.

Performing a non-supervised HCA on all spectra extracted from the micro-BV image acquired with the SR-IR source, two clusters are very well separated as shown in the dendrogram in Fig. 4A, where one cluster corresponds to the surrounding tissue (ST) and the second one to the BV. These spectra were marked in the IR image (defined by PCA from Fig. 2G since it shows clearly the different parts of the micro-BV) and delimit unequivocally the vessel (Fig. 4B). To identify any existing differences in biochemical composition between the two vessels in question, spectra from the vessel wall were compared. Taking only the outer spectra (defining the contour of the micro-BV) as shown in Fig. 4B and also choosing only the spectra of the outer area of the big BV that correspond to the vessel wall *i.e.* tunica externa (Fig. 4C), the resulting vector normalized average spectra were compared in the second derivative with 9 smoothing points. Fig. 4D shows the spectral range of 1750–1600 cm^{-1} which is dominated by the protein content of the vessel wall. The major peak at 1657 cm^{-1} arises from the ν(C═O) stretching vibrations of amide I and shows higher intensity thus higher protein content in the big BV wall with respect to the micro-BV one. Another important peak in this spectral range is 1638 cm^{-1}, which could be attributed to the triple helix of collagen (the major component of the vessel wall especially collagen types I and IV). This peak is higher in intensity in the micro-BV with respect to the big BV. This can be

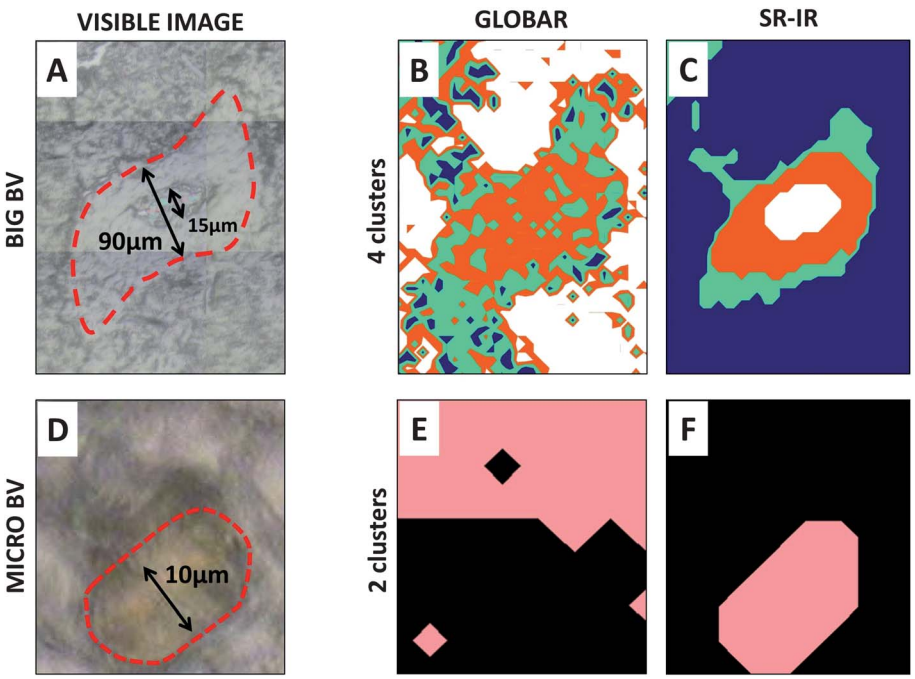

Fig. 3 Representative cluster images of glioma big and micro-BV constructed based on HCA results depending on the used IR source. (A) Visible image of the big BV. (B and C) Corresponding false-color images based on 4 clusters from data acquired with the globar and SR source, respectively. (D) Visible image of the micro BV. (E and F) Corresponding false-color images based on 2 clusters from data acquired with the globar and SR source, respectively.

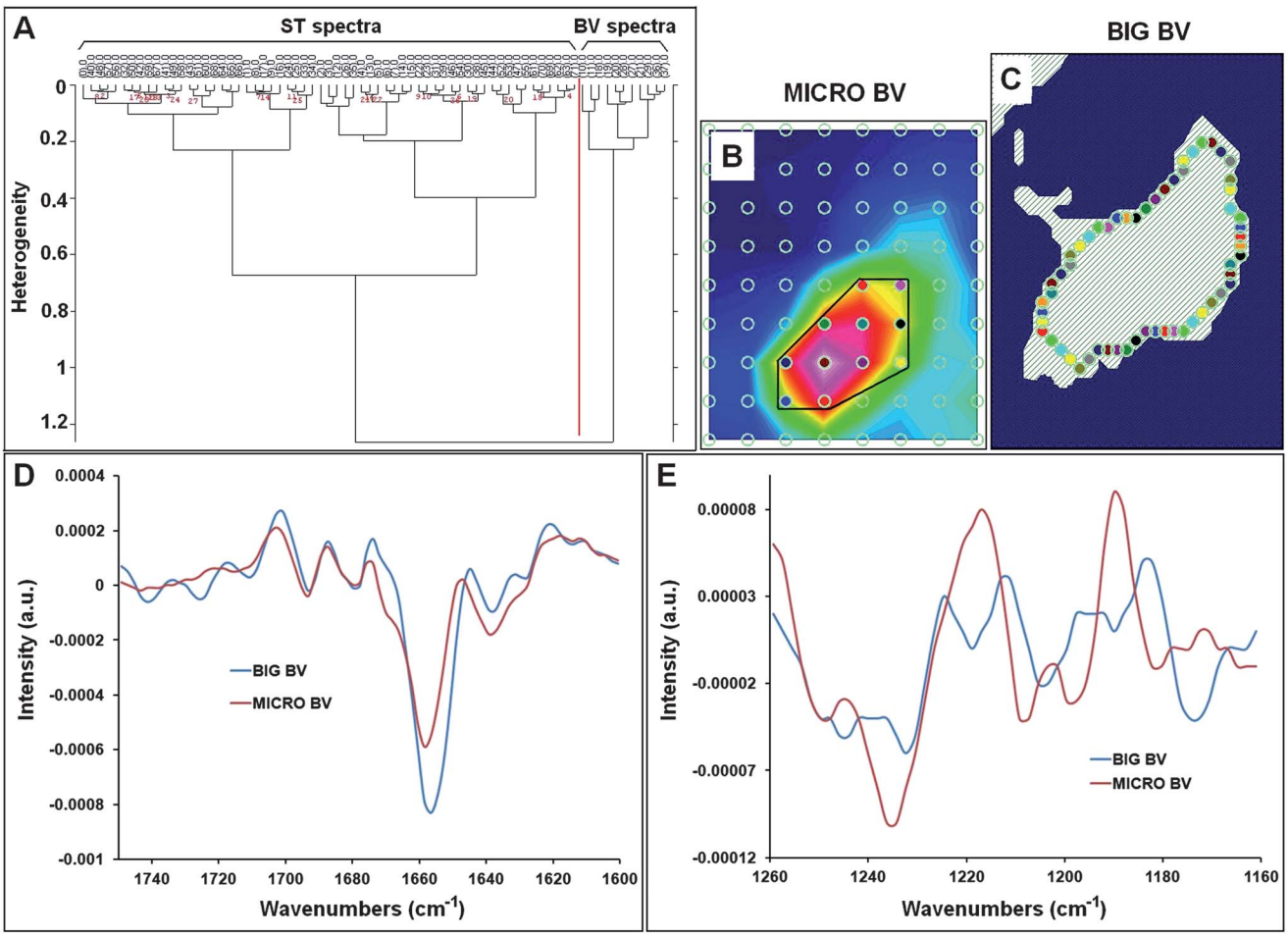

Fig. 4 Comparison between big and micro-BV walls on images acquired with the SR-IR source. (A) Non-supervised HCA on micro-BV spectra ($n = 72$) showing two clusters which correspond to the BV area (BV spectra, $n = 11$) and the surrounding tissue (ST spectra, $n = 61$). (B) Measurement positions of the spectra collected on the micro-BV where a contour is drawn to highlight the spectra given by the BV cluster in A. (C) Spectra positions chosen for the big BV wall ($n = 57$). (D and E) Second derivative of average spectra of the big and micro-BV wall in the spectral range (1750–1600 cm^{-1}) and (1260–1160 cm^{-1}) respectively.

explained by higher contents in collagen type I which has been proven to have higher contents of triple helix than collagen type IV.[34] This peak difference is in concordance with previous results[10] where it has been shown that large BVs reveal a decrease in the triple helix content with respect to small BVs. The spectral range (1260–1160 cm^{-1}) also contains important bands especially at 1233 and 1203 cm^{-1} that could be attributed to collagen (Fig. 4E). As shown in this figure, there is a difference in these peak positions (shifted to 1236 and 1207 cm^{-1}) between the two spectra. This difference could be explained by the structural alteration of collagen and its deformation induced by tumor growth and the angiogenic stress. It is also known that heterogeneity is a common feature of tumor vasculature thus not all tumor vessels exhibit the same organization.

Our results show that a high brilliant SR beam provides very satisfying quality signal compared with the globar source to study spectral images for relevant analysis of BVs from glioma tissues. Indeed, the SR source permits us to obtain a very satisfactory SNR, allowing further relevant investigation of spectral intra- and inter-tissue differences, with a sufficient spatial resolution to allow a clear and unambiguous highlighting of small tissue structures like sub-structure in big BV or micro-BV. In addition, classical curve integration of relevant spectral regions and chemometric analysis *i.e.* PCA/HCA could provide extra information about sub-structure and complement each other to define potential markers specific to BV in the normal or diseased state. Also when comparing the vessel wall spectra for the big and micro-BVs, this gave more information on the collagen structure change due to tumor progression. These results are very promising for characterizing original spectral-based tumoral markers related to the disease state for the purpose of complementing previous findings and having full information on the changes of glioma vasculature.

Conclusion

It is recognized that determining original spectral-based tumoral markers related to biochemical changes of micro-BVs could be of interest for both understanding the underlying mechanisms of glioma development and their clinical management. Therefore, this short study aims to assess

whether IR microspectroscopy using a SR source could provide advantages over a classical globar IR source for detailed spectral analysis of small tissue structures such as glioma micro-BV.

Since bench-top spectrometers are relatively affordable equipment for laboratory, the classical globar source is widely used in IR spectro-imaging research on tumor tissues. These spectrometers are easy to use and permit us to acquire a relatively large area of tissue section. They are also able to provide accurate spectral signal quality for spatial resolution down to 20 μm, allowing us to highlight original tumor markers not detectable by conventional HE or IHC staining. However, when analyzing small tissue structures such as micro-BV for the purpose of extracting spectral features related to disease, globar sources present strong limitations. In this study we show that for spatial resolution less than 10 μm, globar sources confirm not to be sufficiently brilliant to provide an accurate quality signal allowing relevant spectral-based analysis of glioma micro-vessels. On the other hand FTIR imaging using a SR source can provide high quality spectral images, which allows relevant and robust analysis of intra- and inter-tissue spectral differences.

Considering the advantages and inconveniences of SR and globar sources for FTIR imaging, we suggest that these two techniques offer an interesting complementarity when analyzing tumor tissue sections. A globar-IR spectrometer should be used for both screening large tissue components and/or localization of areas of interest, and a SR-IR spectrometer should be used for detailed analysis of small tissue structures and/or previously targeted areas of interest.

Competing interests

The authors have declared that no competing interests exist.

Acknowledgements

This work was supported by EU (proposal SM6019) for beamtime at the MIRIAM beamline of Diamond Light Source, UK. We thank the Pathology Department team at Bordeaux University Hospital for their assistance in performing the tissue sections.

References

1 K. Ali, Y. Lu, U. Das, R. Sharma, S. Wiebe, K. Meguro, V. Sadanand, D. Fourney, A. Vitali, M. Kelly, T. May, J. Gomez and E. Pellerin, *Int. J. Mol. Med.*, 2010, **26**, 11–16.
2 S. Kesari, *Semin. Oncol.*, 2011, **38**, S2–S10.
3 R. Bonavia, M. Inda, W. Cavenee and F. Furnari, *Cancer Res.*, 2011, **71**, 4055–4066.
4 A. Claes, A. Idema and P. Wesseling, *Acta Neuropathol.*, 2007, **114**, 443–458.
5 M. J. Baker, E. Gazi, M. D. Brown, J. H. Shanks, N. W. Clarke and P. Gardner, *J. Biophotonics*, 2009, **2**, 104–113.
6 B. Bird, M. Miljkovic, M. J. Romeo, J. Smith, N. Stone, M. W. George and M. Diem, *BMC Clin. Pathol.*, 2008, **8**, 8.
7 K. T. Cheung, J. Trevisan, J. G. Kelly, K. M. Ashton, H. F. Stringfellow, S. E. Taylor, M. N. Singh, P. L. Martin-Hirsch and F. L. Martin, *Analyst*, 2011, **136**, 2047–2055.
8 D. C. Fernandez, R. Bhargava, S. M. Hewitt and I. W. Levin, *Nat. Biotechnol.*, 2005, **23**, 469–474.
9 G. Bellisola and C. Sorio, *Am. J. Cancer Res.*, 2012, **2**, 1–21.
10 K. Wehbe, R. Pinneau, M. Moenner, G. Deleris and C. Petibois, *Anal. Bioanal. Chem.*, 2008, **392**, 129–135.
11 K. Wehbe, R. Pinneau, S. Eimer, A. Vital, H. Loiseau and G. Déléris, *Analyst*, 2010, **135**, 3052–3059.
12 A. Beljebbar, S. Dukic, N. Amharref, S. Bellefqih and M. Manfait, *Anal. Chem.*, 2009, **81**, 9247–9256.
13 S. Sobottka, K. Geiger, R. Salzer, G. Schackert and C. Krafft, *Anal. Bioanal. Chem.*, 2009, **393**, 187–195.
14 K. Gajjar, L. D. Heppenstall, W. Pang, K. M. Ashton, J. Trevisan, I. I. Patel, V. Llabjani, H. F. Stringfellow, P. L. Martin-Hirsch, T. Dawson and F. L. Martin, *Anal. Methods*, 2013, **5**, 89–102.
15 M. Diem, K. Papamarkakis, J. Schubert, B. Bird, M. Romeo and M. Milkovic, *Appl. Spectrosc.*, 2009, **63**, 307–318.
16 L. Wang and B. Mizaikoff, *Anal. Bioanal. Chem.*, 2008, **391**, 1641–1654.
17 A. Travo, O. Piot, R. Wolthuis, C. Gobinet, M. Manfait, J. Bara, M. Forgue-Lafitte and P. Jeannesson, *Histopathology*, 2010, **56**, 921–931.
18 R. Wolthuis, A. Travo, C. Nicolet, A. Neuville, M. Gaup, D. Guenot, E. Ly, M. Manfait, P. Jeannesson and O. Piot, *Anal. Chem.*, 2008, **80**, 8461–8469.
19 J. Nallala, O. Piot, M.-D. Diebold, C. Gobinet, O. Bouché, M. Manfait and G. D. Sockalingum, *Cytometry, Part A*, 2013, **83**, 294–300.
20 P. Dumas, G. D. Sockalingum and J. Sule-Suso, *Trends Biotechnol.*, 2007, **25**, 40–44.
21 A. Marcelli, A. Cricenti, W. M. Kwiatek and C. Petibois, *Biotechnol. Adv.*, 2012, **30**, 1390–1404.
22 A. Marcelli and G. Cinque, in *Biomedical Applications of Synchrotron Infrared Microspectroscopy*, ed. D. Moss, The Royal Society of Chemistry, 2011.
23 G. Cinque, M. Frogley, K. Wehbe, J. Filik and J. Pijanka, *Synchrotron Radiation News*, 2011, **24**, 24–33.
24 G. Carr, *Rev. Sci. Instrum.*, 2001, **72**, 1613–1619.
25 A. Travo, V. Desplat, E. Barron, E. Poychicot-cousteau, J. Guillon, G. Déléris and I. Forfar, *Anal. Bioanal. Chem.*, 2012, **404**, 1733–1743.
26 P. Lasch, W. Haensch, D. Naumann and M. Diem, *Biochim. Biophys. Acta*, 2004, **1688**, 176–186.
27 L. Dietrich, S. Mellberg, E. Langenkamp, L. Zhang, A. Zieba, H. Salomäki, M. Teichert, H. Huang, P. Edquivst, T. Kraus, H. Augustin, T. Olofsson, E. Larsson, O. Söderberg, G. Molema, F. Pontén, P. Georgii-Hemming, I. Alafuzoff and A. Dimberg, *J. Pathol.*, 2012, **228**, 378–390.
28 M. Miller and P. Dumas, *Biochim. Biophys. Acta*, 2006, **1758**, 846–857.
29 W. Duncan and G. Williams, *Appl. Opt.*, 1983, **22**, 2914–2922.
30 J. Chalmers, N. Everall, K. Hewitson, M. Chasters, M. Pearson, A. Grady and B. Ruzicka, *Analyst*, 1998, **123**, 579–586.

31 M. Miller and R. Smith, *Vib. Spectrosc.*, 2005, **38**, 237–240.
32 I. I. Patel, J. Trevisan, G. Evans, V. Llabjani, P. L. Martin-Hirsch, H. F. Stringfellow and F. L. Martin, *Analyst*, 2011, **136**, 4950–4959.
33 C. Krafft and V. Sergo, *Spectroscopy*, 2006, **20**, 195–218.
34 C. Petibois, G. Gouspillou, K. Wehbe, J. P. Delage and G. Deleris, *Anal. Bioanal. Chem.*, 2006, **386**, 1961–1966.